Journal of Materials Chemistry A

Electron transfer properties of chemically reduced graphene materials with different oxygen content

Journal:	*Journal of Materials Chemistry A*
Manuscript ID:	TA-ART-02-2014-001034.R1
Article Type:	Paper
Date Submitted by the Author:	30-Apr-2014

Complete List of Authors:	Tan, Shu Min; Nanyang Technological University, Division of Chemistry and Biological Chemistry Ambrosi, Adriano; Nanyang Technological University, Chemistry and Biological Chemistry Chua, Chun Kiang; Nanyang Technological University, Chemistry and Biological Chemistry Pumera, Martin; Nanyang Technological University, Chemistry and Biological Chemistry

Journal of Materials Chemistry A RSCPublishing

ARTICLE

Electron transfer properties of chemically reduced graphene materials with different oxygen content

Cite this: DOI: 10.1039/x0xx00000x

Shu Min Tan, Adriano Ambrosi, Chun Kiang Chua and Martin Pumera*

Received 00th January 2012,
Accepted 00th January 2012

DOI: 10.1039/x0xx00000x

www.rsc.org/

Herein, we endeavoured to tune the surface composition and hence electron transfer properties of chemically reduced graphene oxides through varying the mass of sodium borohydride ($NaBH_4$) in the reduction step. The resulting materials were characterised *via* X-ray photoelectron spectroscopy (XPS), Raman spectroscopy, Fourier transform infrared spectroscopy (FTIR), and conductivity studies. The XPS and Raman spectra show positive correlations between the mass of $NaBH_4$ used, and C/O ratios and I_D/I_G ratios of the materials, respectively. The graphene materials exhibit improved conductivity with greater degrees of reduction and FTIR shows that, specifically, carbonyl groups were reduced to hydroxyl groups. The cyclic voltammetry technique was then employed to elucidate a trend between the heterogeneous electron transfer of $Fe(CN)_6^{3-/4-}$, $Ru(NH_3)_6^{2+/3+}$, $Fe^{2+/3+}$, $V^{2+/3+}$, $Eu^{2+/3+}$, ascorbic and uric acids, and the C/O ratios. It was found that the dependency of the heterogeneous electron transfer on oxygen content in chemically reduced graphenes is more complex than previously thought and that multiple concurring effects participate.

1 Introduction

It has been brought to the attention of researchers that graphene, a monolayer of sp^2 carbon atoms packed tightly in a two-dimensional honeycomb lattice, has outstanding mechanical, thermal and electrical conductivity,[1,2] with high specific surface area[3] and rapid heterogeneous electron transfer rates,[4] and can be fabricated easily.[5] Due to its extraordinary properties and relative ease of production, extensive research has been conducted with graphenes displaying promising potential in conductive films,[6] composite materials,[7] electrochemical devices[8] and drug delivery.[9] The fabrication routes can be broadly classified into two categories: bottom-up approach, which utilises the chemical vapour deposition (CVD) technique that prepares graphene sheets from carbon sources like methane,[10] benzene[11] and polymers[11,12]; and top-down approach, which involves the chemical oxidation of graphite, followed by electrochemical reduction,[13,14] or chemical reduction[15-18] using reducing agents like sodium borohydride ($NaBH_4$), or thermal reduction *via* an exfoliation process.[19, 20] Amongst the preparation methods available for graphene, the top-down approach has the highest potential to be up-scaled for industrial production and is generally the preferred method. The thermal exfoliation/reduction method generally subjects the graphite oxide materials to a thermal shock which allows the rapid expansion and hence, exfoliation of graphite oxide,[21] while simultaneously removing molecular oxygen and carbon-oxygen gases,[22] resulting in graphene materials with little to no oxygen-containing groups remaining. The requisite of rapidly increasing temperature of the thermal exfoliation/reduction method requires expensive machinery with highly pure and controlled atmosphere. Further, it would be difficult and complicated to attempt to obtain partial thermal reduction of graphene oxide and control the amount of oxygen functionalities that are left. In general, graphene oxides can be electrochemically reduced using simple instrumentation immediately after modification onto an electrode surface. Though the electrochemical reduction allows control over the extent of reduction of graphene materials,[23] it is ambiguous which groups are being reduced at the applied potential. The long exposure between electrode modification and subsequent

measurements may have altered the graphene materials in undetermined ways.

Currently, of the three common reduction methods, the chemical reduction of graphene oxides is, by far, the most efficient and cost effective reduction technique. Chemically reduced graphene oxides (CRGOs) are generally fabricated by employing reductants like $NaBH_4$ and lithium aluminium hydride ($LiAlH_4$). These reductants and their reduction mechanisms have been widely studied and it is known that some oxygen functionalities are more susceptible to reduction by them.[24] A host of reductants are able to remove a significant amount of oxygen functionalities such as hydroxyl and epoxy (present in basal plane), and carbonyl and carboxylic (present in edges) in graphene oxides,[15-18,25,26] resulting in partial recovery of the aromaticity of the graphene backbone.[27] A previous study by Shin *et al.* investigated the reduction of graphene oxides by $NaBH_4$ and it was clearly shown that the carbonyl groups were reduced to C-O groups which were further reduced with a higher concentration of reductant, together with the removal of some carboxylic groups.[17] Our previous study which compared the reduction of graphene oxides by different reductants showed that $LiAlH_4$ was most effective in reducing carboxylic groups.[26] These methods produce CRGOs with excellent electrical properties, with potential towards bulk production. Hence, CRGOs are generally the preferred and least hassle graphene material.

Previously, we have explored the possibility of tuning the surface composition and electron transfer properties of graphenes *via* electrochemical reduction of graphene oxides.[23] It was discovered that electrochemical reduction was able to tune the amount of surface oxygen residing on the graphene. This opens up the likelihood of preparing graphenes with specific electrochemical properties. Furthermore, with the booming energy and electronics industries and afore stated advantages of CRGOs, they have the potential to be the next emerging electronic and capacitance material with vast applications and simple fabrication routes. This, coupled with the possibility of tuning the electrochemical properties of graphene, makes the inspection of the surface composition and electron transfer properties of graphenes produced *via* chemical reduction of graphene oxide the next important step towards fabricating materials with specific properties required for their functions.

Herein, we wish to investigate the effects of differing C/O ratio on changes in the peak-to-peak separation (ΔE) of various redox couples and oxidative peak potential of biomolecules. The graphene materials of increasing C/O ratios were synthesised by reducing graphene oxide with increasing mass of sodium borohydride ($NaBH_4$). X-ray photoelectron spectroscopy (XPS), Raman spectroscopy, Fourier transform infrared spectroscopy (FTIR) and conductivity studies were used to characterise the materials and confirm the removal of the oxygen functionalities. Due to their differing oxygen content, they show different electrical properties and also different suspension stabilities in *N,N*-dimethylformamide (DMF) solvent. Cyclic voltammetry (CV) was then performed using five different redox probes, $Fe(CN)_6^{3-/4-}$, $Ru(NH_3)_6^{2+/3+}$, $Fe^{2+/3+}$, $V^{2+/3+}$ and $Eu^{2+/3+}$ and two redox active biologically important molecules, ascorbic and uric acid, to elucidate the influence of the oxygen functionalities on the ΔE and oxidative peak potential. The resulting ΔE and oxidation potential varied non-linearly with the variation of the C/O ratio indicating that multiple factors contribute to the electron transfer event, including density of defects, conductivity and aggregation tendency of the materials.

2 Experimental

2.1 Materials

Graphite, sodium borohydride, *N,N*-dimethylformamide (DMF), hydrochloric acid, potassium phosphate dibasic, sodium phosphate monobasic, sodium chloride, and potassium chloride were purchased from Sigma-Aldrich. Sulphuric acid and potassium chlorate were obtained from Alfa Aesar. Fuming nitric acid (>90%) were purchased from J. T. Baker. Potassium hexacyanoferrate(III), potassium hexacyanoferrate(II) trihydrate, hexaammineruthenium(III) chloride, iron(III) chloride hexahydrate, europium(III) nitrate pentahydrate, vanadium(III) chloride, *L*-ascorbic acid and uric acid were obtained from Sigma-Aldrich. Sodium carbonate, and the glassy carbon (GC) electrodes, Ag/AgCl electrode and platinum (Pt) electrode were purchased from Sinopharm and CH Instruments respectively. Milli-Q water with resistivity of 18.2 MΩ cm was utilised throughout for the preparation of solutions.

2.2 Apparatus

X-ray photoelectron spectroscopy (XPS) measurements were performed using a conventional non-monochromated X-ray source using the Mg Kα line (SPECS XR50, $h\upsilon$ = 1253 eV, 200 W) and a multichannel energy analyser (SPECS Phoibos 100 MCD-5). Survey and high-resolution C1s core-level spectra were collected. Relative atomic percentages were used to evaluate of C/O ratios from survey XPS spectra. XPS samples were prepared by coating a uniform layer of the relevant material onto conductive carbon tape. Raman spectroscopy analyses were conducted using a confocal micro-Raman LabRam HR instrument from Horiba Scientific in backscattering geometry with a CCD detector, a 514.5 nm Ar laser and a 100× objective attached to an Olympus optical microscope. Prior to the measurements, a calibration was made using an internal silicon reference at 520 cm^{-1} and a peak position resolution of less than 1 cm^{-1} was obtained. The spectra ranged from 1000 to 3000 cm^{-1}. The Fourier transform infrared spectroscopy (FTIR) measurements were conducted using an attenuated total reflectance method on a PerkinElmer Spectrum 100 system. A diamond/ZnSe was used as the ATR crystal in tandem with a universal ATR accessory. Current–voltage measurements (*I–V* curve) were obtained using an interdigitated gold electrode platform (Au-IDE) by depositing 2 μL of the material suspension (1 $mgmL^{-1}$ dispersed in water) onto the electrode surface with 10 μm spacing.[41] The electrode

was then left under a lamp to dry, leaving a randomly deposited material film on the interdigitated area that linked the two Au electrode bands. The *I–V* curves were acquired by linear sweep voltammetric measurements at a scan rate of 20 mVs^{-1}. An average from three measurements was obtained and displayed in Figure 4. The electrochemical experiments employing the cyclic voltammetric technique were conducted using a μAutolab Type III electrochemical analyzer (Eco Chemie, The Netherlands) connected to the software NOVA 1.8 (Eco Chemie).

2.3 Procedures

2.3.1 Graphite oxide (GO). GO was prepared from graphite according to Staudenmaier method.[29] Sulphuric acid (17.5 mL, 95–98%) and nitric acid (fuming, 9 mL) were added to a round bottom flask and stirred under 0 °C for 15 min. Graphite (1 g) was then added into the mixture under vigorous stirring to avoid agglomeration and to obtain a homogeneous dispersion. Subsequently, potassium chlorate (11 g, 89.8 mmol) was added portionwise into the mixture (over 15 min) at 0 °C. The mixture was stirred for 96 h at room temperature. Upon completion of the reaction, the mixture was poured into deionised water (1 L) and filtered. Graphite oxide was then dispersed and rinsed repetitively with HCl (5%) solutions to eliminate sulphate ions and finally washed with ultrapure water until the pH of the reaction mixture matches that of the ultrapure water. The graphite oxide slurry was then dried in vacuum at 40 °C for 5 days.

2.3.2 Reduced graphene oxides (rGO-x, x = mass of $NaBH_4$). Graphite oxide (50 mg) dispersed in ultrapure water (1.0 $mgmL^{-1}$) was ultrasonicated (Fischer-brand, FB 11203 ultrasonic unit at 37 kHz, 180 W) for 2 h before adding 5 wt% of sodium carbonate to obtain a colloidal suspension of pH 9−10. Sodium borohydride (50 mg, 1.32 mmol; 100 mg, 2.64 mmol; 300 mg, 7.93 mmol; 800 mg, 21.1 mmol) was added slowly (over 20 min) into the suspension under vigorous stirring. The mixture was then heated to 80 °C for 1 h. It was cooled to room temperature, filtered (0.2 μm, RC membrane) and washed repeatedly using ultrapure water. The sample was then dried in vacuum at 40 °C for 5 days before usage.

2.3.3 Electrochemical characterisation of materials. GO, rGO-50, rGO-100, rGO-300 and rGO-800 (1.0 $mgmL^{-1}$) were individually dispersed in DMF for 1 h prior to usage. Before the modification of the glassy carbon (GC) electrode, its surface was polished to a mirror finish using 0.05 mm alumina particles on a polishing pad. After sonication for 10 min, 1 μL aliquot of the materials suspension was drop cast onto a newly polished GC electrode surface with a micropipette. To achieve a randomly distributed graphene film on the GC surface, the graphene material suspension was allowed to dry under a lamp. All cyclic voltammetric (CV) measurements were performed using a scan rate of 100 mVs^{-1}, in a 5 mL electrochemical cell at room temperature. A three-electrode configuration comprising of the modified GC working electrode, Ag/AgCl reference electrode and Pt counter electrode was employed. Phosphate buffered solution (PBS, 50 mM, pH 7.2) was utilised as the supporting electrolyte for the biomolecules while potassium chloride (KCl, 0.1 M) was the electrolyte for the redox couples. Triplicate CV measurements were performed for all materials.

3 Results and Discussion

Previous study on the change in Δ*E* of the redox peaks of the ferro/ferricyanide redox couple ($Fe(CN)_6^{3-/4-}$) with graphene materials of different oxygen content has exhibited a negative correlation between C/O ratio and Δ*E*.[28] To investigate whether the results from these studies can be extended to other redox couples and biomolecules, we firstly characterised the graphene materials by means of XPS, Raman spectroscopy, FTIR and conductivity and then performed CV to obtain Δ*E* and oxidative peak potentials. The graphene materials used are namely graphene oxide produced using the Staudenmaier[29] oxidation method (denoted as GO) and GO reduced with 50, 100, 300 and 800 mg of $NaBH_4$ (denoted as rGO-x, whereby x is the mass of $NaBH_4$ (in grams) used in the reduction step). Note that rGO-800 is more commonly known as fully chemically reduced graphene oxide (CRGO) and the use of lower amounts of $NaBH_4$ results in graphenes with decreasing C/O ratios as confirmed by XPS.

XPS, a surface-sensitive technique which is able to identify surface elemental composition of the graphene materials, was performed to obtain the C/O ratio for GO, rGO-50, rGO-100, rGO-300 and rGO-800. Figure 1A shows the wide scan XPS spectra of the materials, with two prominent peaks at 284.5 and 531.3 eV, corresponding to carbon and oxygen respectively.

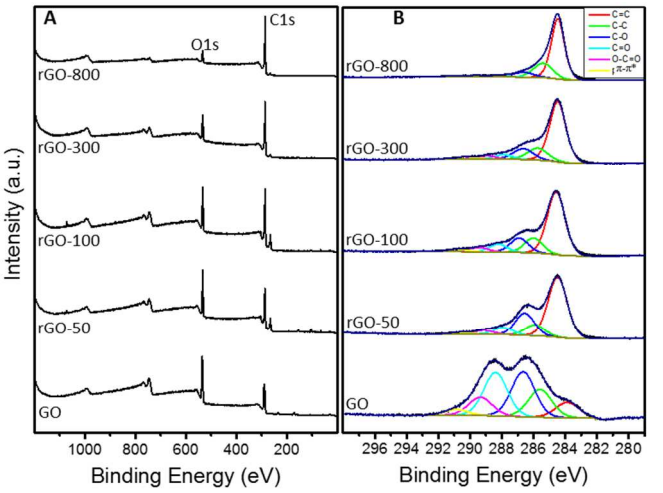

Figure 1 X-ray photoelectron spectroscopy spectra of GO, rGO-50, rGO-100, rGO-300 and rGO-800. (**A**) Survey and (**B**) C1s core-level spectra.

The C/O ratio of each material, calculated from the atomic percentages obtained from the wide scan spectra, reveals that the C/O ratio varies positively with $NaBH_4$ mass. GO presented the lowest C/O ratio of 2.0, followed by rGO-50 with C/O of 2.6, rGO-100 with C/O of 3.5, rGO-300 with C/O of 4.8 and rGO-800 with the highest C/O ratio of 9.5. GO contains a large amount of oxygen-containing groups stemmed from the Staudenmaier oxidation reaction giving a low C/O ratio. The other materials, reduced with increasing amounts of $NaBH_4$

showed increased C/O ratios mainly due to the elimination/reduction of carbonyl groups on the graphene carbon backbone. The C1s core-level XPS spectra of the different graphene materials are presented in Figure 1B. The deconvolution of the C1s spectra revealed peaks corresponding to sp^2 C=C (284.5 eV), sp^3 C-C (285.5 eV), hydroxyl/epoxide C-O (286.5 eV), carbonyl C=O (about 288.0 eV), carboxylic O-C=O (about 289.0 eV) and π-π* shake-up (about 290.5 eV) for all the materials. The π-π* shake-up peaks are common for conjugated materials and occur as a result of additional electronic transitions following a photoelectron emission process. From Figure 1B, the peaks for the various carbon-oxygen bonds diminish from GO to rGO-800 while the peak for C=C bond shows the opposite trend. It is typical for graphene oxides to partially recover the sp^2 carbon network after being chemically reduced.[27]

Further structural characterisation was performed using Raman spectroscopy, a technique useful for measuring the density of defects present in the sp^2 honeycomb structure of carbon materials. The Raman spectrum usually shows two peaks characteristic of carbon materials; D band at about 1350 cm^{-1}, which originates from structural disorders and sp^3-like defects in the backbone, and G band at about 1580 cm^{-1}, which originates from sp^2-hybridised carbon vibrations. An analysis of the ratio of the intensities of D band to G band (I_D/I_G) can be used to examine the extent of defects in graphenes after reduction. The Raman spectra for GO and rGO-x are displayed in Figure 2. The I_D/I_G ratios of GO, rGO-50, rGO-100, rGO-300 and rGO-800 were obtained to be 0.89, 0.92, 0.98, 1.13 and 1.68 respectively. The increase in the I_D/I_G ratio with greater degree of reduction of graphene oxide is consistent with previous reports.[30-32] The increase in I_D/I_G ratio is indicative of the reduced sp^2 lattice size (L_a) on graphenes upon reduction. It has been proposed[30] that while reduction decreases the size of the sp^2 domains, it increases their number all over the material which causes the enhanced conductivity. Therefore, though the reduction of graphene oxide results in recovery of graphene backbone, this is confined to small graphitic regions, hence a larger I_D/I_G ratio is obtained.

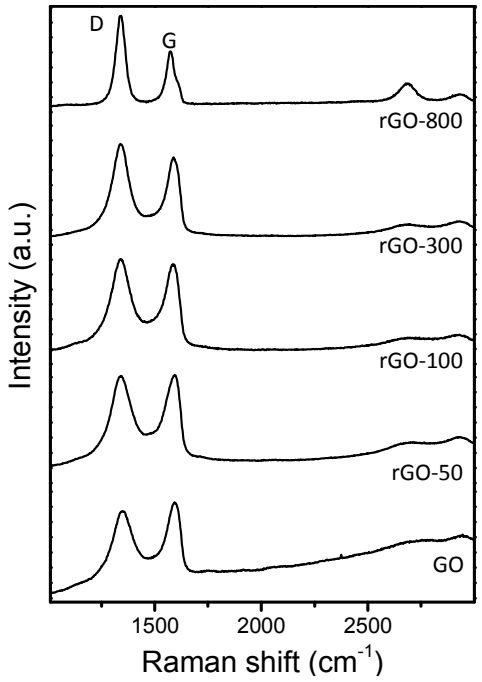

Figure 2 Raman spectra for GO, rGO-50, rGO-100, rGO-300 and rGO-800.

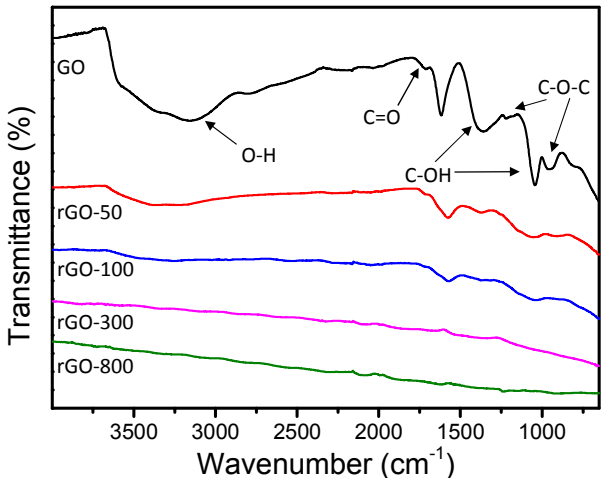

Figure 3 FTIR spectra of GO, rGO-50, rGO-100, rGO-300 and rGO-800.

FTIR spectroscopy was performed to further elucidate the oxygen functionalities residing on GO and rGO-x and the spectra are found in Figure 3. As it can be seen, the spectrum for the GO material presents several peaks which correspond to the O-H stretching mode (~3200 cm^{-1}), C=O vibrational mode (~1720 cm^{-1}), C-OH vibrational mode (~1360 and ~1050 cm^{-1}) and C-O-C from epoxides (1220 and 950 cm^{-1}). The peak at ~1620 cm^{-1} corresponds to the vibrational mode of adsorbed water molecules.

It is clear looking at the FTIR spectra of the reduced materials that carbonyl groups are reduced by $NaBH_4$ since the C=O peak diminishes until it is no longer detected for rGO-300 and rGO-800. At larger mass of the reductant, the O-H, C-OH and C-O-C groups were reduced as well, as shown in the respective disappearing peaks from the FTIR spectra. This is in agreement with the C1s core-level XPS spectra (Figure 1B) which shows decreasing C-O peaks from GO to rGO-800, and with literature whereby more $NaBH_4$ led to the reduction of C-O bonds[17] that may correspond to hydroxyl or epoxide groups. The reduction of carbonyl groups to hydroxyl groups by $NaBH_4$ is consistent with conventional organic chemistry.[24]

In addition to the structural characterisations *via* XPS, Raman and FTIR spectroscopic techniques as mentioned above, electrical properties of the graphene materials were investigated through conductivity studies. An interdigitated gold electrode system was employed to measure conductivities of all the materials. For each material, this system provides *I-V* curves (Figure 4) with slopes that are directly proportional to their

individual conductivities. This enables direct qualitative comparison of conductivities of the materials.

From Figure 4, conductivities increase from GO to rGO-50, followed by rGO-100, rGO-300 and rGO-800. GO and rGO-50 showed similar and negligible conductivities due to high sheet resistance as a result of the many oxygen-containing groups residing on the graphene sheet ($R>10^4$ Ω). rGO-800 which was the most highly reduced graphene, displayed the steepest slope of 64 mAV^{-1} (R=15.6 Ω), followed by rGO-300 with slope of 52.8 mAV^{-1} (R=18.9 Ω) and rGO-100 with slope of 31.4 mAV^{-1} (R=31.8 Ω). These results are indicative that a greater degree of GO reduction has led to improved electrical properties of the resulting reduced graphene.

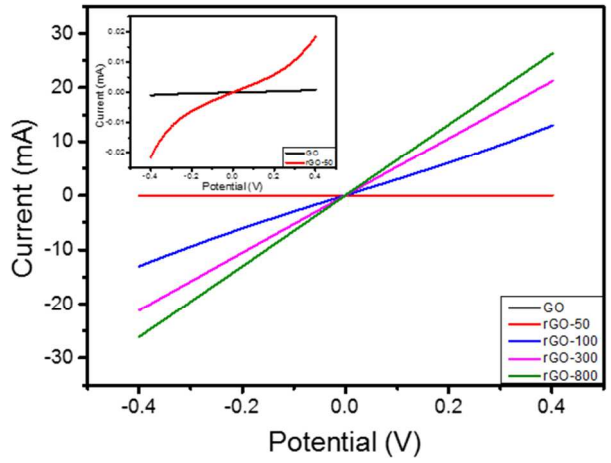

Figure 4 *I-V* curves of GO, rGO-50, rGO-100, rGO-300 and rGO-800. Inset: *I-V* curves of GO and rGO-50 only.

We also tested the stability of the graphene materials in the organic solvent DMF which was used to prepare graphene dispersions prior to electrode surface modification. Figure 5 shows optical images of colloidal suspensions of GO and rGO-x, immediately after sonication ($t = 0$) and after 1, 4, 24, 94 and 168 h. It can be seen that the rGO-300 and rGO-800 are much less stable than the other materials given the fact that they settle to the bottom of the vial sooner. The aggregation is due to the removal of dissociable oxygen containing groups from the surface of rGO and consequently reduced stabilising surface charges.

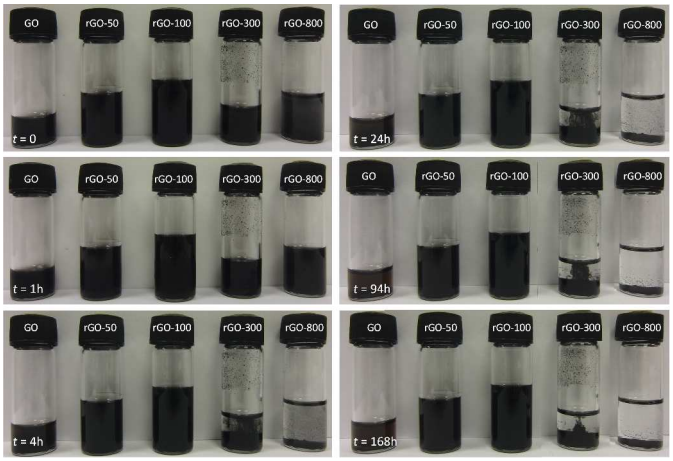

Figure 5 Optical images of GO, rGO-50, rGO-100, rGO-300 and rGO-800 dispersions in water at time *t* after sonication.

Finally, we explored the electrochemical properties of GO and rGO-x using CV technique in the presence of various redox couples and biomolecules, i.e. $Fe(CN)_6^{3-/4-}$, $Ru(NH_3)_6^{2+/3+}$, $Fe^{2+/3+}$, $V^{2+/3+}$, $Eu^{2+/3+}$, ascorbic and uric acids. While $Fe(CN)_6^{3-/4-}$, $Ru(NH_3)_6^{2+/3+}$, $Fe^{2+/3+}$, $V^{2+/3+}$ and $Eu^{2+/3+}$ are redox probes typically used to investigate electrochemical properties of the materials including their heterogeneous electron transfer ability, ascorbic and uric acids are biologically important molecules and are used here to test the biosensing capabilities of the various materials when used as electrode surface modifiers.

Figure 6 and 7 show the CVs obtained for the redox probes and biomolecules respectively. The $Ru(NH_3)_6^{2+/3+}$ redox couple, which is likened to an "outer-sphere" redox system, has been shown to be surface, as well as oxide, insensitive. Here, in fact, gave relatively stable and reproducible ΔE values across graphenes with different oxygen content and density of defects. Compared to $Ru(NH_3)_6^{2+/3+}$, the other redox couples were greatly influenced by the amount of oxygen-containing groups in the graphenes, as shown in the variability of the shape of the CVs. From Figure 7, uric acid shows relatively stable response, in terms of peak potential, to the different graphenes with varying C/O ratios, while ascorbic acid gave more complex responses with oxidation potentials varying not linearly with the C/O ratio.

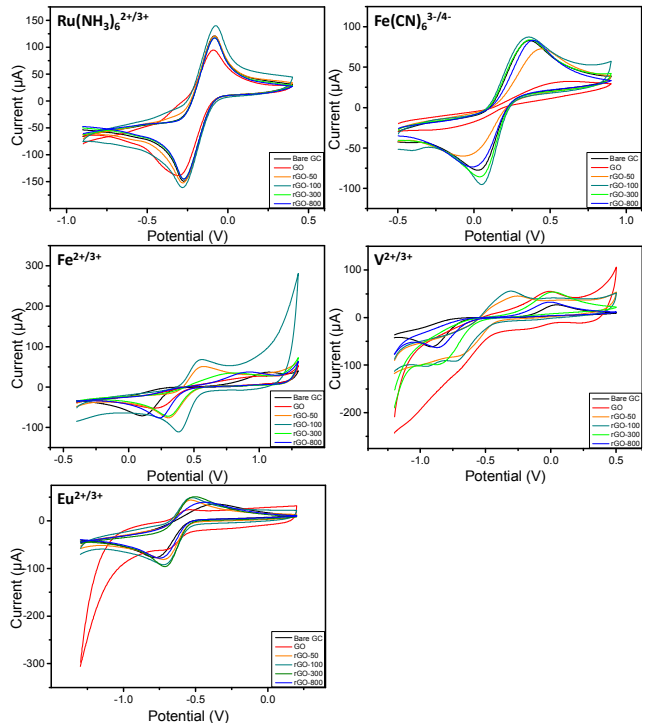

Figure 6 Cyclic voltammograms of various redox couples on bare glassy carbon, GO, rGO-50, rGO-100, rGO-300 and rGO-800. All probes were dissolved in potassium chloride solution (0.1 M) to form 10 mM solutions. Scan rate used was 100 mVs^{-1}.

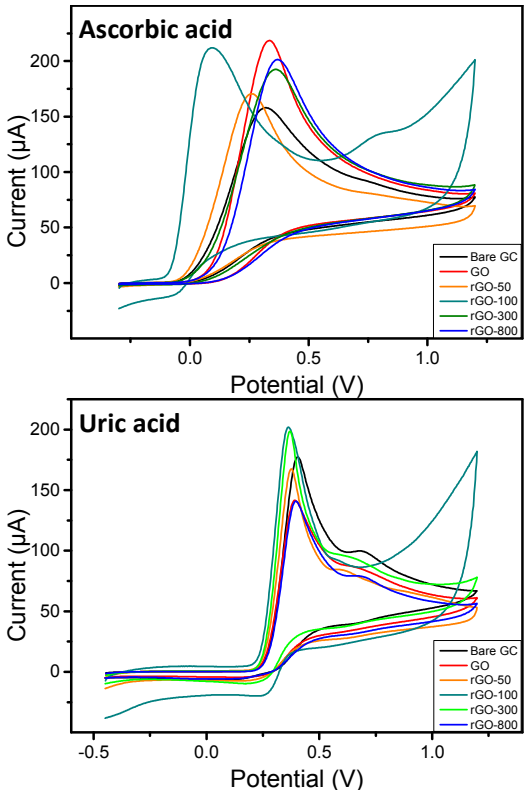

Figure 7 Cyclic voltammograms of ascorbic and uric acids on bare glassy carbon, GO, rGO-50, rGO-100, rGO-300 and rGO-800. All probes were dissolved in phosphate buffer solution (50 mM, pH 7.2) to form 10 mM solutions. Scan rate used was 100 mVs^{-1}.

For a better visualisation and understanding of the influence of oxygen functionalities, ΔE and oxidation potentials have been plotted against C/O ratios of the materials (Figure 8 and 9). Due to its insensitivity to oxides and surface defects, $Ru(NH_3)_6^{2+/3+}$ showed very stable electrochemical responses (change in ΔE = 0.02 V) across the graphenes with increasing C/O ratios. On the other hand, $Fe(CN)_6^{3-/4-}$ showed in general a diminished ΔE, with increasing C/O ratios. This corresponds to earlier reports demonstrating that a faster electron transfer for $Fe(CN)_6^{3-/4-}$ is obtained at reduced oxygen content due to the weaker electrostatic repulsion between dissociated oxygen groups and the negatively charged $Fe(CN)_6^{3-/4-}$.[28,31] In addition, the accelerated electron transfer of $Fe(CN)_6^{3-/4-}$ can be correlated to the increased density of defects of the materials, as demonstrated in previous studies.[33]

As for $Fe^{2+/3+}$ and $V^{2+/3+}$, the correlation between ΔE and C/O ratio is not linear. In both cases, in fact, it can be noticed a decreasing ΔE from GO to rGO-100 (C/O ratio from 2.0 to 3.5), followed by a constant increase at increasing C/O ratios from 3.5 to 9.5. This clearly highlights that the surface oxides are not the only factor influencing the electron transfer of these redox probes with the carbon material. For perfectly controlled carbon surfaces, the HET of $Fe^{2+/3+}$, $V^{2+/3+}$ and $Eu^{2+/3+}$ is strongly influenced by surface oxides which accelerate the electron transfer due to favourable interactions between such oxides and the redox probes.[34] Here we can see that for $Fe^{2+/3+}$ and $V^{2+/3+}$ probes, the initial decrease of oxygen groups going from GO to rGO-100 generates an enhanced electron transfer with diminished ΔE which contradicts earlier reports. We infer that for such oxygen functionalities-rich materials the conductivity plays the major role with respect to the C/O ratio. GO and rGO-50 are in fact poorly conductive with only rGO-100 starting to have an ohmic behaviour (see Figure 4). From this point onwards, having the rest of the materials increasing but comparable conductivities, the oxygen functionalities seemed to have the main influence towards the redox behaviour of $Fe^{2+/3+}$ and $V^{2+/3+}$ probes, with therefore poorer electron transfer for reduced oxygen content.

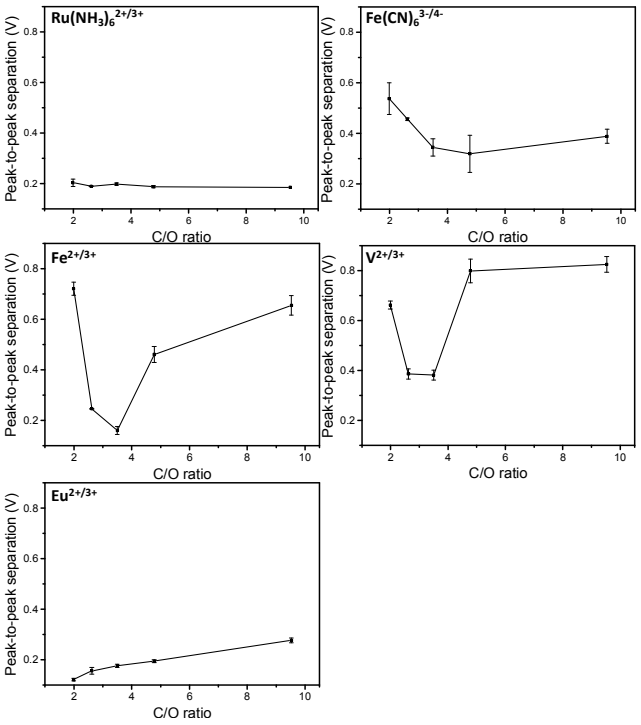

Figure 8 Peak-to-peak separations (Δ*E*) of various redox couples against C/O ratios of GO, rGO-50, rGO-100, rGO-300 and rGO-800 obtained from XPS. Error bars indicate triplicate measurements and the y-axes were scaled to a uniform range.

On the other hand it is surprising that $Eu^{2+/3+}$ displayed a more monotonic behaviour with smaller, but observable positive correlation between Δ*E* and C/O ratio. Clearly the electron transfer mechanism involved with $Eu^{2+/3+}$ follows different paths with the oxygen content being the only influencing factor. Δ*E* for $Eu^{2+/3+}$ in fact, monotonically increased with increased removal of oxygen containing groups. This is consistent with the previous observation that $Eu^{2+/3+}$ ligates with oxygen containing groups on the carbon surfaces.[35, 36] While it is expected to have similar redox mechanism between $Fe^{2+/3+}$, $V^{2+/3+}$ and $Eu^{2+/3+}$ (coordination to oxygen functionalities in graphene), from the CVs obtained, it seems that $Fe^{2+/3+}$ and $V^{2+/3+}$ do have similar mechanisms, while $Eu^{2+/3+}$ differ from them. This may be due to the larger size of the Eu atom compared to V and Fe, whereby larger atomic size indicates lower charge density and weaker ligation to oxygen-containing groups. Hence, oxygen content in graphene becomes a limiting factor in the observed trend.

The oxidation mechanism of ascorbic acid has been well-examined over the last few decades.[37,38] It was determined that ascorbic acid undergoes electrochemical oxidation at sites of "pristine" carbon.[38] From Figure 9, the electrochemical oxidation potential of ascorbic acid decreases initially to a minimum for rGO-100, after which it increases for rGO-300 and rGO-800. With reduction by $NaBH_4$, it is possible that the recovery of the aromaticity of graphene backbone has occurred, which was supported by the increasing peak height of C=C bond in the C1s core-level spectra. Hence, the electrochemical oxidation of ascorbic acid proceeded *via* the active sites of sp^2 hybridised carbon on graphene and lower oxidative peak potentials were observed. However, considering the Raman spectra, a substantial increase of the I_D/I_G ratio resulted for the rGO-100 to rGO-800 passing from the value 0.98 to the value 1.68. This indicated a significant disruption of the "pristine" graphene backbone which might have led to the increase in the oxidative peak potential.

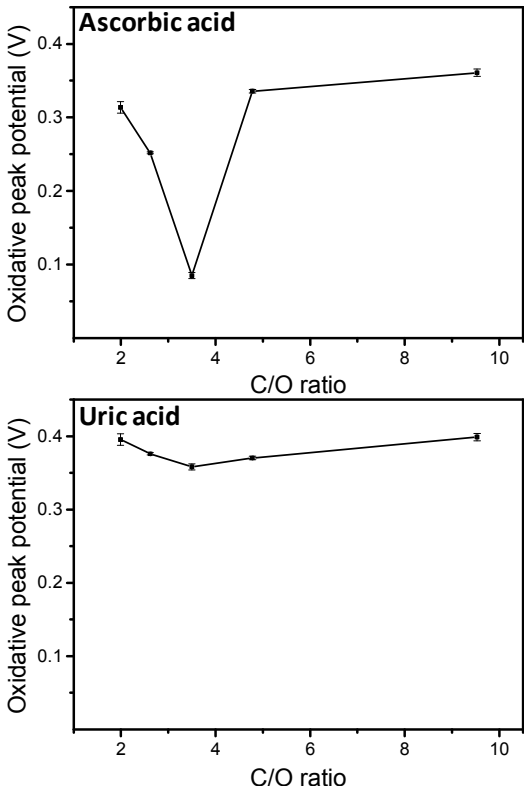

Figure 9 Oxidative peak potentials of ascorbic and uric acids against C/O ratios of GO, rGO-50, rGO-100, rGO-300 and rGO-800 obtained from XPS. Error bars indicate triplicate measurements and the y-axes were scaled to a uniform range.

The variation of the oxidation potential with C/O ratio for uric acid is much less significant if compared to that of ascorbic acid with a potential shift of only ~0.04 V. Such minimal variation agrees with earlier studies which revealed that the electrochemical behavior of uric acid is mostly affected by the presence of metal impurities, as well as by the solution pH.[39, 40] In the present study neither of these factors were varied and only the C/O ratio of the materials was considered.

4 Conclusion

CRGOs with specific surface composition and electrochemical properties have been successfully prepared by reducing graphene oxides with varying masses of $NaBH_4$, resulting in differing C/O ratios. The variation of Δ*E* and oxidative peak potentials of redox couples and biomolecules with differing C/O ratios was investigated, and various trends were observed. Both $Ru(NH_3)_6^{2+/3+}$ and uric acid have shown to be unaffected by differing oxygen contents. $Fe(CN)_6^{3-/4-}$ shows overall

decreasing ΔE with C/O ratio due to the removal of negatively charged oxygen functionalities. $Fe^{2+/3+}$ and $V^{2+/3+}$ probes, however, are affected not only by the surface oxides but also by other factors with the major being the electrical conductivity. For highly oxidised materials, an improved electron transfer is mostly attributable to the improved conductivity properties of the materials while reducing the oxygen functionalities. After that having comparable conductivities, the oxides interaction prevails giving rise to poorer electron transfer at increased C/O ratios. $Eu^{2+/3+}$ shows differing behavior with a constant increase in ΔE for decreasing amount of oxygen containing groups at the carbon surface to which it can bond. Ascorbic acid oxidation potential decreased at increasing C/O ratios up to rGO-100 probably due to the recovery of the aromaticity and conductivity of the graphene backbone. Subsequently, the increase in oxidation potential is probably due to the higher amount of defects which reduce the pristine graphene surfaces available for interaction. Uric acid, although with similar trend as ascorbic acid, results in much less significant alteration of the ΔE at varying C/O ratio, conductivity and density of defects. This study allows the fabrication of graphene materials with specific surface composition and electron transfer properties, which is an imperative step towards their use in specific applications.

Acknowledgements

M.P. acknowledges Tier 2 grant (MOE2013-T2-1-056; ARC 35/13) from Ministry of Education, Singapore.

Notes and references

1 K. S. Novoselov, A. K. Geim, S. V. Morozov, D. Jiang, Y. Zhang, S. V. Dubonos, I. V. Grigorieva and A. A. Firsov, *Science*, 2004, **306**, 666-669.
2 A. K. Geim, *Science*, 2009, **324**, 1530-1534.
3 M. D. Stoller, S. Park, Y. Zhu, J. An and R. S. Ruoff, *Nano Lett.*, 2008, **8**, 3498-3502.
4 W. Cai, Y. Zhu, X. Li, R. D. Piner and R. S. Ruoff, *Appl. Phys. Lett.*, 2009, **95**, 123115-123117.
5 A. Martín, J. Hernandez-Ferrer, L. Vazquez, M.-T. Martínez, A. Escarpa, *RSC Adv*., 2014, **4**, 132.
6 K. S. Kim, Y. Zhao, H. Jang, S. Y. Lee, J. M. Kim, K. S. Kim, J.-H. Ahn, P. Kim, J.-Y. Choi and B. H. Hong, *Nature*, 2009, **457**, 706-710.
7 S. Stankovich, D. A. Dikin, G. H. B. Dommett, K. M. Kohlhaas, E. J. Zimney, E. A. Stach, R. D. Piner, S. T. Nguyen and R. S. Ruoff, *Nature*, 2006, **442**, 282-286.
8 a) M. Pumera, A. Ambrosi, A. Bonanni, E. L. K. Chng and H. L. Poh, *Trends Anal. Chem.*, 2010, **29**, 954-965. b) A. Martín, A. Escarpa. *Trends Anal. Chem.* 2014, **56**, 13.
9 Z. Liu, J. T. Robinson, X. Sun and H. Dai, *J. Am. Chem. Soc.*, 2008, **130**, 10876-10877.
10 H. Zhou, W. J. Yu, L. Lin, R. Cheng, Y. Chen, X. Huang, Y. Liu, Y. Wang, Y. Huang and X. Duan, *Nat. Commun.*, 2013, **4**, 2096.
11 Z. Li, P. Wu, C. Wang, X. Fan, W. Zhang, X. Zhai, C. Zeng, Z. Li, J. Yang and J. Hou, *ACS Nano*, 2011, **5**, 3385-3390.
12 Z. Sun, Z. Yan, J. Yao, E. Beitler, Y. Zhu and J. M. Tour, *Nature*, 2010, **468**, 549-552.
13 M. S. Goh and M. Pumera, *Electroanalysis*, 2012, **24**, 1147-1152.
14 J. Yang and S. Gunasekaran, *Carbon*, 2013, **51**, 36-44.
15 C. K. Chua and M. Pumera, *J. Mater. Chem. A*, 2013, **1**, 1892-1898.
16 Z. Lei, L. Lu and X. S. Zhao, *Energy Environ. Sci.*, 2012, **5**, 6391-6399.
17 H.-J. Shin, K. K. Kim, A. Benayad, S.-M. Yoon, H. K. Park, I.-S. Jung, M. H. Jin, H.-K. Jeong, J. M. Kim, J.-Y. Choi and Y. H. Lee, *Adv. Funct. Mater.*, 2009, **19**, 1987-1992.
18 U. Hofmann and E. Konig, *Z. Anorg. Allg. Chem.*, 1937, **234**, 311-336.
19 H. L. Poh, F. Šaněk, A. Ambrosi, G. J. Zhao, Z. Sofer and M. Pumera, *Nanoscale*, 2012, **4**, 3515-3522.
20 Y. Zhu, S. Murali, W. Cai, X. Li, J. W. Suk, J. R. Potts and R. S. Ruoff, *Adv. Mater.*, 2010, **22**, 3906-3924.
21 M. J. McAllister, J. L. Li, D. H. Adamson, H. C. Schniepp, A. A. Abdala, J. Liu, M. Herrera-Alonso, D. L. Milius, R. Car, R. K. Prud'homme and I. A. Aksay, *Chem. Mater.*, 2007, **19**, 4396-4404.
22 R. Larciprete, S. Fabris, T. Sun, P. Lacovig, A. Baraldi and S. Lizzit, *J. Am. Chem. Soc.*, 2011, **133**, 17315-17321.
23 A. Ambrosi and M. Pumera, *Chem. Eur. J.*, 2013, **19**, 4748-4753.
24 M. B. Smith and J. March, *March's Advanced Organic Chemistry; Reactions, Mechanisms, and Structure*, John Wiley & Sons, Inc., Hoboken, New Jersey, 2007.
25 X. Fan, W. Peng, Y. Li, X. Li, S. Wang, G. Zhang and F. Zhang, *Adv. Mater.*, 2008, **20**, 4490-4493.
26 A. Ambrosi, C. K. Chua, A. Bonanni and M. Pumera, *Chem. Mater.*, 2012, **24**, 2292-2298.
27 C. K. Chua and M. Pumera, *Chem. Soc. Rev.*, 2013, **42**, 3222-3233.
28 X. Ji, C. E. Banks, A. Crossley and R. G. Compton, *Chem. Phys. Chem.*, 2006, **7**, 1337-1344.
29 L. Staudenmaier, *Ber. Dtsch. Chem. Ges.*, 1898, **31**, 1481-1487.
30 S. Stankovich, D. A. Dikin, R. D. Piner, K. A. Kohlhaas, A. Kleinhammes, Y. Jia, Y. Wu, S. T. Nguyen and R. S. Ruoff, *Carbon*, 2007, **45**, 1558-1565.
31 C. K. Chua, A. Ambrosi and M. Pumera, *J. Mater. Chem.*, 2012, **22**, 11054-11061.
32 C. K. Chua and M. Pumera, *Chem. Eur. J.*, 2013, **19**, 2005-2011.
33 A. Ambrosi, A. Bonanni and M. Pumera, *Nanoscale*, 2011, **3**, 2256-2260.
34 C. A. McDermott, K. R. Kneten and R. L. McCreery, *J. Electrochem. Soc.*, 1993, **140**, 2593-2599.
35 M. Pumera, M. Cabala, K. Veltruská, I. Ichinose and J. Tang, *Chem. Mater.*, 2007, **19**, 6513-6517.
36 M. Pumera, *Chem. Asian J.*, 2009, **4**, 250-253.
37 D. Njus, M. Wigle, P. M. Kelley, B. H. Kipp and H. B. Schlegel, *Biochemistry*, 2001, **40**, 11905-11911.
38 D. Njus, M. Wigle, P. M. Kelley, B. H. Kipp and H. B. Schlegel, *Biochemistry*, 2001, **40**, 11905-11911.
39 M. Chao, X. Ma and X. Li, *Int. J. Electrochem. Sci.*, 2012, **7**, 2201-2213.
40 M. Griffiths, *J. Biol. Chem.*, 1952, **197**, 399-407.
41 J. Wang, J. Dai and T. Yarlagadda, *Langmuir*, 2005, **21**, 9-12.

